DEVELOPMENT OF ANTENNA-COUPLED METAL-INSULATOR-METAL
DIODES FOR INFRARED DETECTION

BY

ARDY WINOTO

THESIS

Submitted in partial fulfillment of the requirements
for the degree of Master of Science in Electrical and Computer Engineering
in the Graduate College of the
University of Illinois at Urbana-Champaign, 2015

Urbana, Illinois

Adviser:

Professor Milton Feng

Abstract

The long-wavelength infrared (LWIR) band between 7 and 14 μm is significant for thermal imaging purposes because it coincides with the blackbody radiation peak of the human body and a low absorption window in the earth's atmosphere. Also, at 10 μm wavelength, the earth's terrestrial radiation is maximized and provides a good opportunity for untapped energy harvesting. These two factors combine to make a very strong need for a low-cost detector that operates at room temperature in this band. Antenna-coupled metal-insulator-metal (ACMIM) diodes are a leading candidate due to their high speed and potential manufacturability on Si substrates. In this work, Ni-NiO-Ni ACMIM diodes are fabricated using a two-step lithography process and an oxygen plasma oxidation. The device is characterized to both have current in the nA range and responsivities nearing 1000pA/W.

Acknowledgments

First, I would like to thank my advisor Prof. Milton Feng for his guidance and support through the development of ACMIM diodes. Next, I thank AMI Research and Development, LLC, for their support of this project, particularly Patricia Bodan, Benjamin Mcmahon, and William Mouyos for their technical contributions to this work. I would like to thank my mentor Huiming Xu for starting this project and trusting me to continue its development. Also, I thank my HSIC colleagues Eric Iverson, Rohan Bambery, Fei Tan, Mong-Kai Wu, Michael Liu, Curtis Wang, and Junyi Qiu for always being there to help me. Lastly, I dedicate this thesis to my parents, my sister, and my brother who have shown me nothing but never-ending support in my life and academic career.

Contents

1. Introduction

1.1 Motivation

The purpose of this work is to develop a low-cost, room-temperature detector that operates at the long-wavelength infrared (LWIR) band, specifically at 10.6 μm wavelength. This band is significant for three reasons. First, the LWIR band around 7-14 μm contains the peak radiation spectrum for objects at temperatures around 300K, such as the human body. Second, there is very little absorption in the earth's atmosphere in this band. The first two reasons combined make the LWIR band a very suitable candidate for personnel detection applications using IR imaging. Not only does the desired signal peak at the band of interest, but any detector operating in this band has an inherent advantage for long-range detection due to the low atmospheric attenuation. The third reason is that the earth's terrestrial radiation peaks around 10 μm wavelength. While energy from solar radiation in the visible spectrum can be efficiently harvested using photovoltaic junction solar cells with common semiconductor substrates such as Si and GaAs, that technology is not applicable in the LWIR band where most semiconductors are transparent. This means that the LWIR band is relatively untapped for energy harvesting purposes and there is a great demand for a detector that can efficiently convert energy from terrestrial radiation.

IR detectors that operate in the LWIR band can be classified into three categories based on their operating mechanisms. The first is thermal-based IR detectors such as thermopiles, bolometers, and pyroelectric detectors. These detectors operate through thermally-induced changes in the material property such as conductivity and electrical potential due to IR irradiation. Usually a large range of wavelengths can induce thermal change on a given material, so these detectors can operate in a wide wavelength range. However, these are sensitive to the temperature of their surroundings and may require some thermal insulation for the most accurate results. Also, these devices are relatively slow because they are limited by heat conduction.

The second type of detector is a quantum-based detector. These detectors operate through excitation of electrons in a semiconductor substrate as a result of photon absorption. The LWIR band corresponds to transition energies of 0.09 – 0.2 eV where most widely used semiconductors such as Si and GaAs are transparent. Therefore this application requires either semiconductors with very narrow bandgaps such as HgCdTe or a specially designed superlattice structure that favors intersubband transitions at the desired IR wavelength. Photodetectors that utilize such superlattice structures are commonly called quantum well infrared photodetectors (QWIPs). These detectors are much faster than thermal detectors because they rely on electron excitation rather than thermal conductivity. The biggest problem for this type of detector, apart from the high material cost, is the fact that such minute energy transitions easily occur at room temperature through thermal excitation. To reduce noise, these devices generally require cooling to cryogenic temperatures.

The third type of detector is an electromagnetic radiation-based detector. These detectors treat incident light as an electromagnetic wave that is received by an antenna. The antenna couples the electromagnetic radiation to a rectifying element such as a diode to produce an output that corresponds to the incident light. These detectors do not require cooling and operate best in a narrow band around the antenna's design frequency. The speed of one of these detectors is dictated by its rectifying element. This work focuses on an electromagnetic radiation-based detector in the shape of a high speed metal-insulator metal (MIM) diode coupled to a bowtie antenna.

1.2 Antenna-Coupled Metal-Insulator-Metal Diodes

This section discusses the antenna-coupled metal-insulator-metal (ACMIM) diodes, including the tunneling principle behind MIM diodes, previous work in the literature, and design considerations involved in this work.
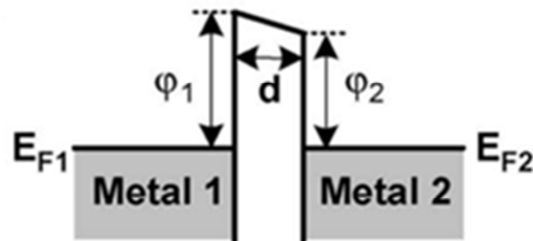
1.2.1 ACMIM Diodes in Literature

Figure 1. Simplified energy band diagram of MIM diodes [1].

A simplified energy band diagram for an MIM diode is shown in Figure 1 [1]. An MIM diode is formed when a thin insulator layer of thickness d is sandwiched between two metals with metal work functions ϕ_1 and ϕ_2, respectively. At equilibrium, Fermi energies E_{F1} and E_{F2} are aligned and the insulator barrier prevents current conduction from Metal 1 to Metal 2. When a bias is applied, one side of the metal is pushed down and the top of the barrier adopts a sharper triangular shape. Using a simple model, the tunneling current through an MIM junction as a function of bias can be expressed as

$$I = cAVe^{-b\varphi^{0.5}d} \tag{1}$$

where ϕ is the barrier height, d is the oxide thickness, A is the junction area, and b and d are constants.
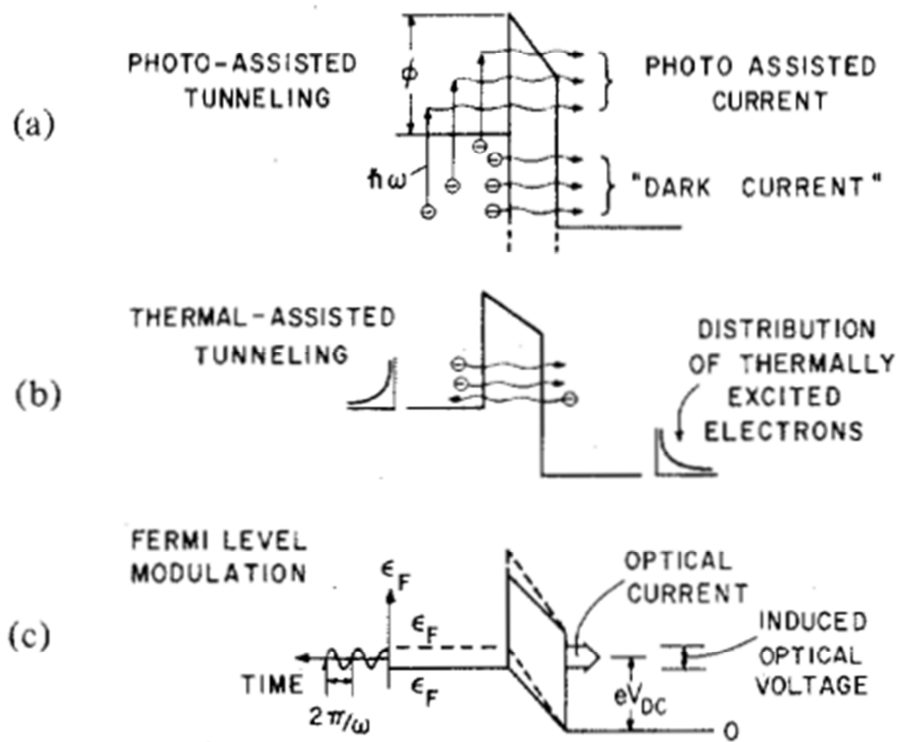
THREE MAJOR PHENOMENA:

Figure 2. Three major phenomena for current conduction in an MIM diode according to Heiblum et al. [2].

Heiblum et al. [2] theorized three major phenomena for current conduction through an MIM junction as illustrated in Figure 2. The first mechanism (a) is photo-assisted tunneling where an electron in the metal near the barrier absorbs a photon with energy $\hbar\omega$ that allows it to reach a point where the barrier is thinner and the tunneling probability greater. When a bias is applied, more electrons can surmount enough energy to tunnel through and the current is increased. This process is fast and depends linearly on the junction area. The second mechanism (b) is called thermal-assisted tunneling. In this case, incoming photons are coupled to phonons, leading to an increase in the metal temperature. Fermi electrons gain additional energy and thus the tunneling current increases. This process is slow and not related to the junction area. The third mechanism (c) is field-assisted tunneling or Fermi-level modulation. If the diode is coupled to an antenna, an electric field is enhanced in the barrier and the Fermi level of the metal will oscillate across a quiescent point at the applied frequency. Because of this

4

field enhancement, the effect of any applied bias to the junction is increased, resulting in a sharper, thinner triangular barrier and a higher probability of electrons to directly tunnel through. Field-assisted tunneling is expected to be the dominant conduction mechanism in ACMIM diodes. Nagae estimates that with an oxide thickness of less than 2nm, the electron transition time is less than 10^{-15} s [3].

The earliest documented work on an MIM tunneling diode was in 1966 [4] for a point contact diode between a tungsten wire antenna with a sharp oxidized tip and a metal surface. These devices provided insight into the operation of MIM tunnel junctions but their mechanical traits made them impractical. In the 1970s, 'edge' thin-film MIM diodes were fabricated on semiconductor wafer substrates [5]. These devices were patterned using optical lithography and the MIM junction was confined to a side opening between two metal layers. Most recently, work has been done at the University of Central Florida on Ni-NiO-Ni ACMIM diodes operating at visible frequencies [6], the University of Notre Dame on Al-AlOx-Pt ACMIM diodes at 10.6μm [7,8], and the University of Maryland on Ni-NiO-Ni ACMIM diodes using the geometric field enhancement technique [1,9].

1.2.2 ACMIM Diodes in This Work

This work focuses on Ni-NiO-Ni MIM diodes coupled to bowtie antennas designed to operate at 10.6 μm by Benjamin McMahon from AMI Research and Development, LLC. The choice of material is made for two reasons. First, nickel is cheap, widely available, and easy to deposit using evaporation techniques. Second, nickel is very slow to oxidize at room temperature, which allows for a controlled oxidation in a two-step lithography process. This thesis focuses on the fabrication process and measurement effort of the ACMIM diodes.

2. Fabrication of ACMIM Diodes

2.1 Substrate

The antenna-coupled MIM diodes are fabricated on a single-side polished p-type Si wafer with 500µm thickness in the <100> orientation from University Wafer. The bare Si surface has a specified resistivity of 0.001-0.005 Ω-cm. A 500nm layer of thermal oxide is grown on the polished Si surface in order to prevent current flow between the top and bottom metal layers through the low-resistance Si substrate.

2.2 Alignment Mark Definition

The first step in ACMIM diode fabrication is the definition of metal alignment marks for subsequent e-beam and optical lithography processes. First, the Si wafers are cleaved into 1 cm^2 pieces. Since the feature size of a single MIM diode is very small (around 0.012 mm^2 including contact pads), a 1 cm^2 die is sufficient to carry enough devices for a given experiment. The wafers are then subjected to a standard solvent bath of acetone, methanol, and IPA to clean off any impurities and organic residue from the surface. A 5 minute dehydration bake at 125°C is performed to evaporate the solvents.

After sample cleaning, the wafer is spin-coated with a layer of PMGI SF11 photoresist (PR) for 60 seconds at 4000rpm. Edge bead removal is performed using a swab and EBR PG solvent to alleviate natural PR buildup at the edges of the wafer. The sample is then allowed to cure on a hotplate for 5 minutes at 225°C. A second PR layer of BPRS-100 is spin-coated for 30 seconds at 4000 rpm followed by a 1 minute soft bake at 110°C and edge bead removal using a swab and acetone. The two different PR layers are exposed by different wavelengths and developed by different developer solutions. The purpose of this bilayer stack is to enable the formation of an undercut between the top and bottom

layer resists. This undercut prevents metal from being deposited on the PR sidewalls, enabling much cleaner liftoff compared to a single layer PR stack.

The next step is UV exposure using a Karl Suss MJB3 Contact Mask Aligner. The mask aligner has a mercury light source and emits light at 320nm wavelength with a fixed intensity of 9mW/cm^2. A quartz-chrome photomask is used to expose the top layer BPRS-100 PR for 25 seconds. Next, the sample is developed using PLSI positive resist developer diluted 1:10 with deionized (DI) water for 40 seconds. Afterwards, a second exposure is done for the bottom layer PMGI SF11. In this case, exposure is done using a flood expose tool based on the OAI Deep Ultraviolet (DUV) Model 30 Light Source. DUV flood exposure is done for 2 minutes at a power level of 1000W. Since the light incident on the sample is collimated, a fused silica UV diffuser is placed on top of the sample to enable light to arrive at the PR opening from multiple angles, promoting the formation of an undercut. After DUV exposure, the sample is developed for 30s in Microchem 101A developer. The DUV exposure and 101A development is repeated one more time to increase undercut depth. Finally, an oxygen plasma descum is done for 30s at 150mT pressure and 250W plasma power using a Diener Tetra 30 Plasma Cleaner to clean off excess PR residue.

A Denton e-beam evaporation system is used to deposit the metal alignment marks. The evaporator consists of an evaporation chamber connected to a helix Cryotorr-8 cryopump which pumps down the chamber to 1e-7 Torr, an e-beam power supply, and an electron gun. Ti, Pt, Au, and Ni metal targets are placed in a 4-pocket rotating stage with samples suspended directly above. An electron beam is focused onto the selected pocket, heating the metal to evaporation point and depositing the evaporated metal onto the sample. A layer of 20nm Ti / 150nm Au is deposited with the metal thickness monitored by a crystal-based deposition monitor. Finally, the excess metal is removed using a 2-step liftoff process. First, the sample is submerged in acetone for 15 minutes at 90°C to remove the BPRS-100

followed by a methanol rinse. Next, the sample is submerged in 1165 microposit remover for 15 minutes at 90°C to remove the PMGI SF11 followed by a methanol and IPA rinse.

2.3 ACMIM Diode Formation

The formation of the ACMIM diode begins with e-beam writing of the bottom bowtie metal layer. The wafer is spin-coated with MMA EL13 e-beam copolymer resist for 1 minute at 5500 rpm followed by a 2 minute cure at 200°C. The top layer resist layer is formed by spin-coating PMMA A2 950 for 1 minute at 2000 rpm followed by a 2 minute cure at 200°C. Since the sample does not come into contact with a physical mask, edge bead removal is not necessary. E-beam exposure is done using a JEOL JBX-6000FS electron beam lithography system. The system is equipped with a thermal field emission gun with ZrO/W emitter and is capable of 50kV acceleration voltage with 10nm resolution and <40nm stitching error. The sample is mounted on a cassette which is transferred into the system through a loadlock and exposed with a current of 100pA.

After exposure, the sample is developed for 105 seconds in a solution of 1:3 MIBK:IPA. Since the bottom layer resist (MMA EL13) is more sensitive than the top layer resist (PMMA A2 950), an undercut profile is automatically formed after a single round of exposure and development. A 30 second oxygen plasma descum is performed before 60nm of nickel is deposited on the sample using e-beam evaporation. Lift-off is done with a methylene chloride bath at 90°C for 15 minutes followed by a methanol/IPA rinse.

The most crucial step in the fabrication of the ACMIM diode is the formation of a thin insulator layer on top of the bottom metal. Several different methods were attempted to achieve this, namely atomic layer deposition (ALD) of aluminum oxide (Al_2O_3), DI water oxidation, and oxygen plasma oxidation. Between these three methods, Oxygen plasma oxidation was found to be the most

reproducible and gave the highest yields. Plasma oxidation is performed using the Diener Tetra 30 Plasma Cleaner. The tool is a barrel etcher which uses concentric reactive ion etching (RIE) to remove thin layers of organic residue. Due to the working principle of the tool, it can also be utilized to controllably oxidize a nickel surface. The tool operates at room temperature without external cooling and a constant pressure of 150mT. The low-frequency RF power can be tuned from 250W to 1kW.

ACMIM diodes were fabricated using different RF power levels and oxidation times. It was found that the best yields are achieved with high plasma power (1kW) and low exposure time (30-45s). Before starting an oxidation process, a plasma chamber clean is done for 5 minutes at 1kW. The sample is placed in the middle of the plasma cleaner and the sample is oxidized for the selected time period. Although nickel oxidizes very slowly at room temperature, it is best to oxidize the sample immediately following bottom metal liftoff to minimize native oxidation in ambient conditions.

Once the bottom metal layer has been oxidized, the sample must be coated with the bilayer e-beam resist stack as soon as possible so as to minimize excess exposure to air. Top metal definition follows the same exact procedure as that for the bottom metal. Since the ACMIM diodes have very small overlap areas, precise alignment between the top and bottom metal layers is important. Figure 3 below shows an example of various overlap sizes that occur on different parts of the wafer when alignment is not done properly.
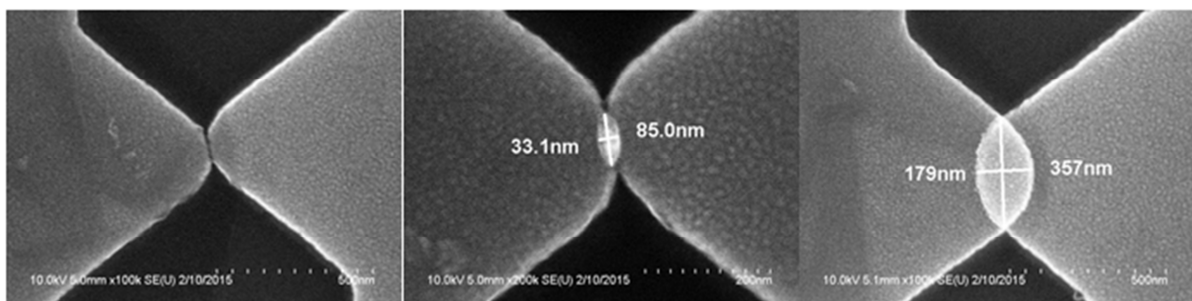
Figure 3. Overlap areas in a single ACMIM diode ranging from no overlap (left) to an overlap area of 0.2μm^2.

Afterwards, metal contact pads are deposited using the exact same procedure as alignment mark deposition. The only difference is that since the bottom contact arm is covered with nickel oxide, a direct contact deposition would form a diode between the contact arm and the contact pad. Therefore, the contact deposition is preceded by a 10 second etch in 40% HCl to remove the oxide layer. A contact pad of 20nm Ti / 180nm Au is deposited followed by a standard acetone-1165 liftoff process.
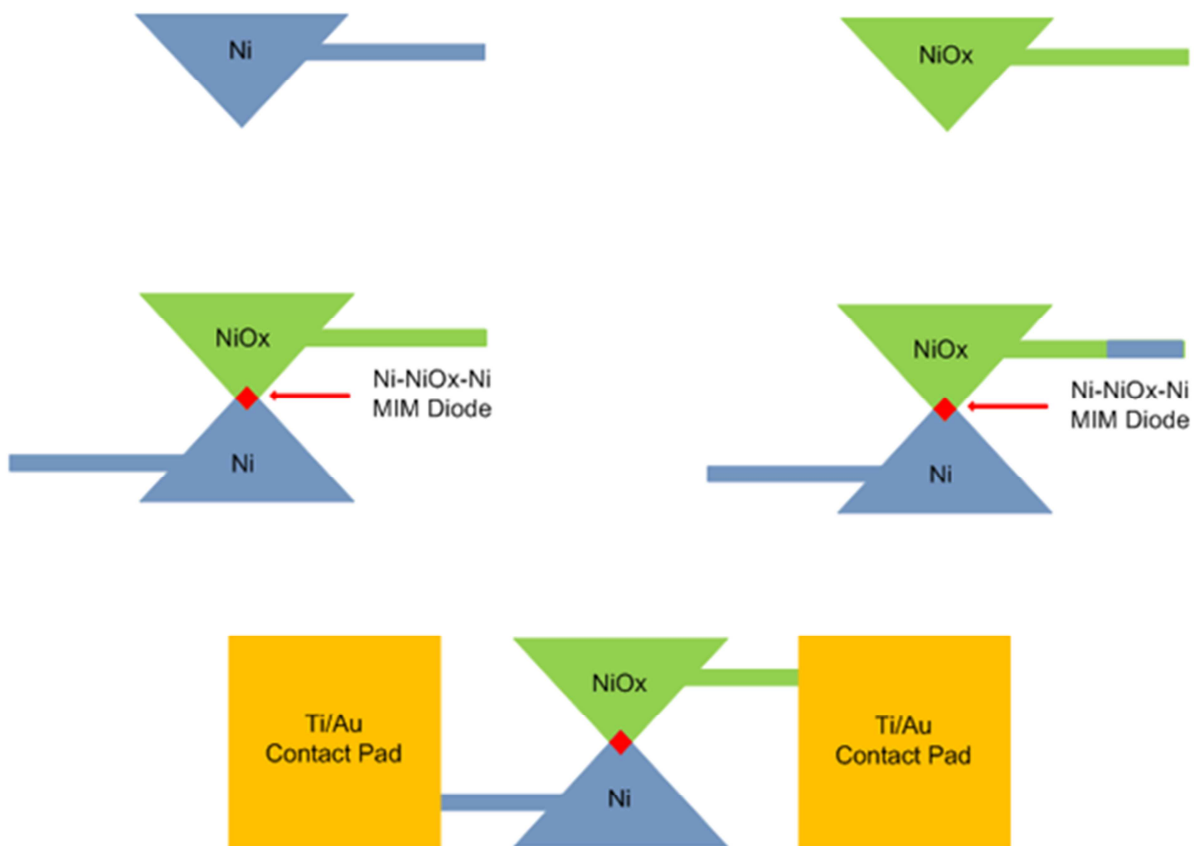

Figure 4. Process flow for ACMIM diode formation.

The process steps specific for the Ni-NiOx-Ni Bowtie MIM Rectenna are illustrated in Figure 4. It is possible to fabricate a Bowtie MIM Rectenna using an arbitrary set of bottom and top metal layers while still using a NiOx insulator, which is favorable because its slow native oxidation rate allows for a more controlled process. Such a device would require the deposition of a thin Ni layer over the bottom metal layer. The entire thin Ni layer can then be oxidized using RIE such that a metal-NiO bottom layer is

obtained. Note that partial oxidation of the Ni layer will result in a metal-Ni-NiO bottom layer.

Afterwards, an arbitrary top metal layer may be deposited without any additional complexity followed

by contact pad deposition.
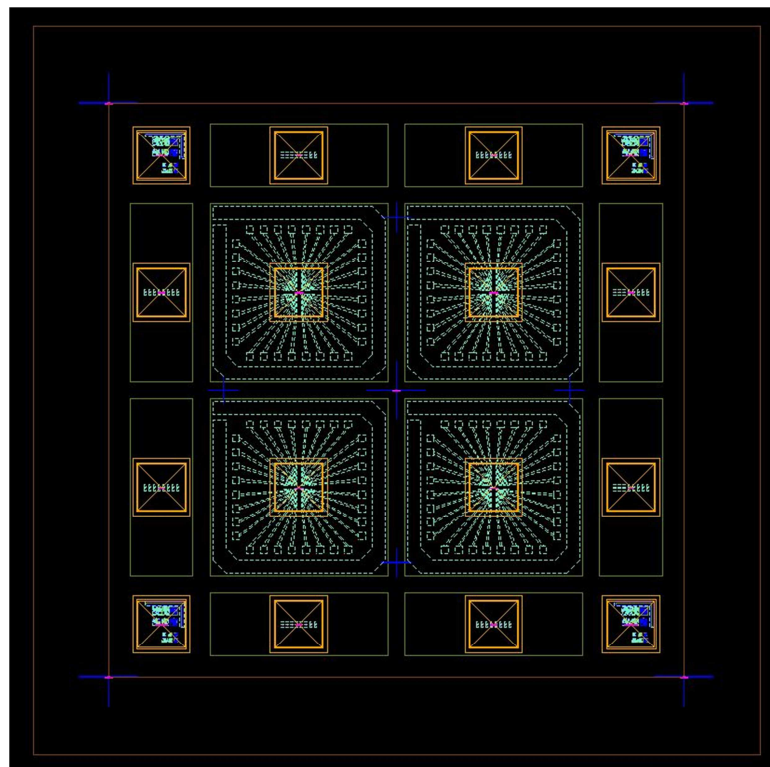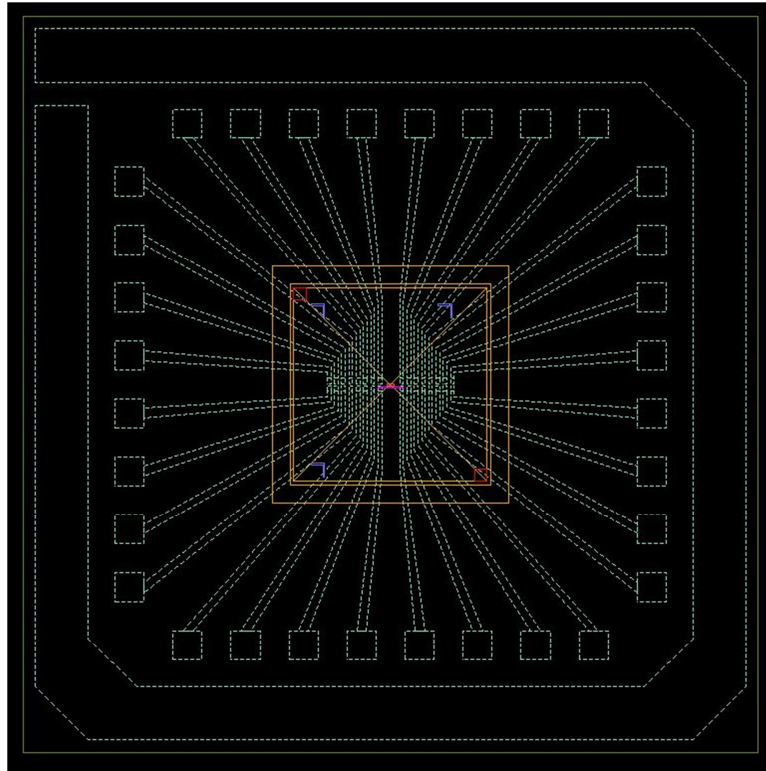
2.4 Mask Layout and Chip Packaging

Figure 5. ACMIM diode die mask layout.

Figure 6. Close-up view of ACMIM diode chip.

The mask layout used in the ACMIM diode process is shown in Figures 5 and 6. The mask consists of four chips containing identical arrays of 16 ACMIM diodes. Each device is connected to contact pads meant for wire bonding to a chip carrier. Additionally, 8 process control monitor (PCM) structures are located on the edges of the mask. Each PCM structure contains an array of 8 ACMIM diodes for DC testing purposes.

The processed wafer needs to be cut into four individual chips using a dicing saw prior to packaging. The process of cutting a layer of SiO2 generally produces a lot of dust that may affect the performance of the device. Hence, the SiO2 needs to be etched away except around the device area. A masking pattern is first defined using optical lithography with only BPRS-100. After exposure and development, the wafer is hard baked for 2 minutes at 110°C. Then the wafer is submerged in 40% HF for 3 minutes to etch the oxide layer, using the BPRS as a mask. The wafer dicing is using a DiscoDAD

dicing saw with a Nickel blade. Since the vacuum holes on the tool are 2.5" apart, the wafer must first be mounted onto a 4" carrier Si wafer. The wafer bonding is done using a heat-sensitive wax called Crystalbond 501. The Crystalbond is applied to the carrier wafer on a 125°C hotplate until a thin film of melted Crystalbond is formed. The sample wafer is then pressed onto the film and the whole assembly is allowed to cool. After dicing, the carrier wafer is placed on the hotplate to melt the Crystalbond and excess Crystalbond on the sample die is removed using acetone.

Each ACMIM diode needs to have electrical contact to the electrical measurement system while at the same time allowing a controlled light source to illuminate the device. A simple probe station setup cannot be used in this case. To accommodate such needs, the chip is mounted on a 44-pin ceramic leaded chip carrier (CLCC). Each chip is adhered to a 44-pin CLCC using double-sided carbon tape. Wire bonds are made between the contact pads on the die and the contact pads using a Kulicke and Soffa Model 4142 ball bonder. Figure 7 shows the wire bonds on the ACMIM diode chip and the finished CLCC package. To connect the CLCC to measurement instrument, a custom PCB was designed to hold a 44-pin CLCC socket (Figure 8). The two pins that correspond to top and bottom metal contacts of each device are connected to SMA connectors. With this configuration, the device can be connected directly to measurement instrument using a coaxial cable. The finished ACMIM diode package is mounted on a micropositioner stage in Figure 8.
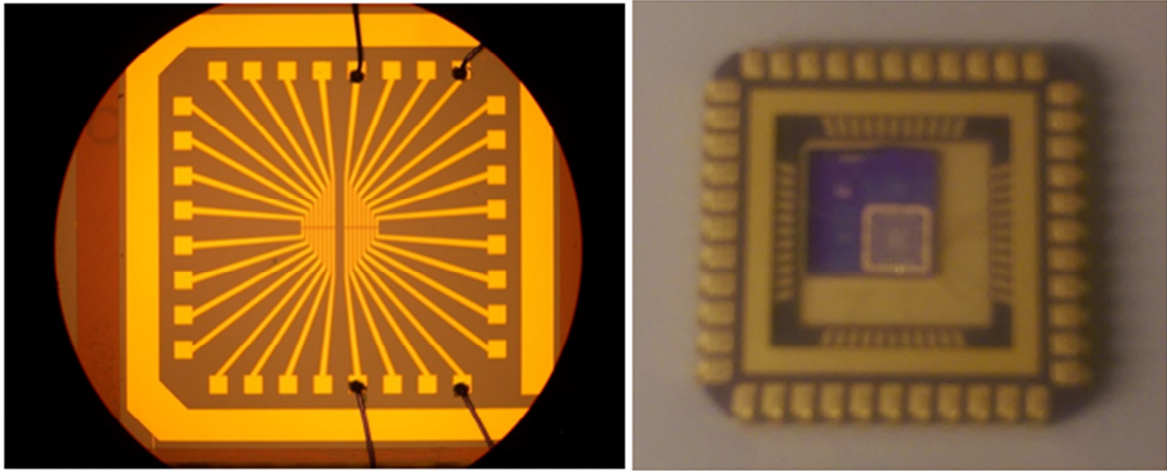
Figure 7. Left: Micrograph of ACMIM diode chip showing wire bonds. Right: ACMIM diode chip mounted on a CLCC.
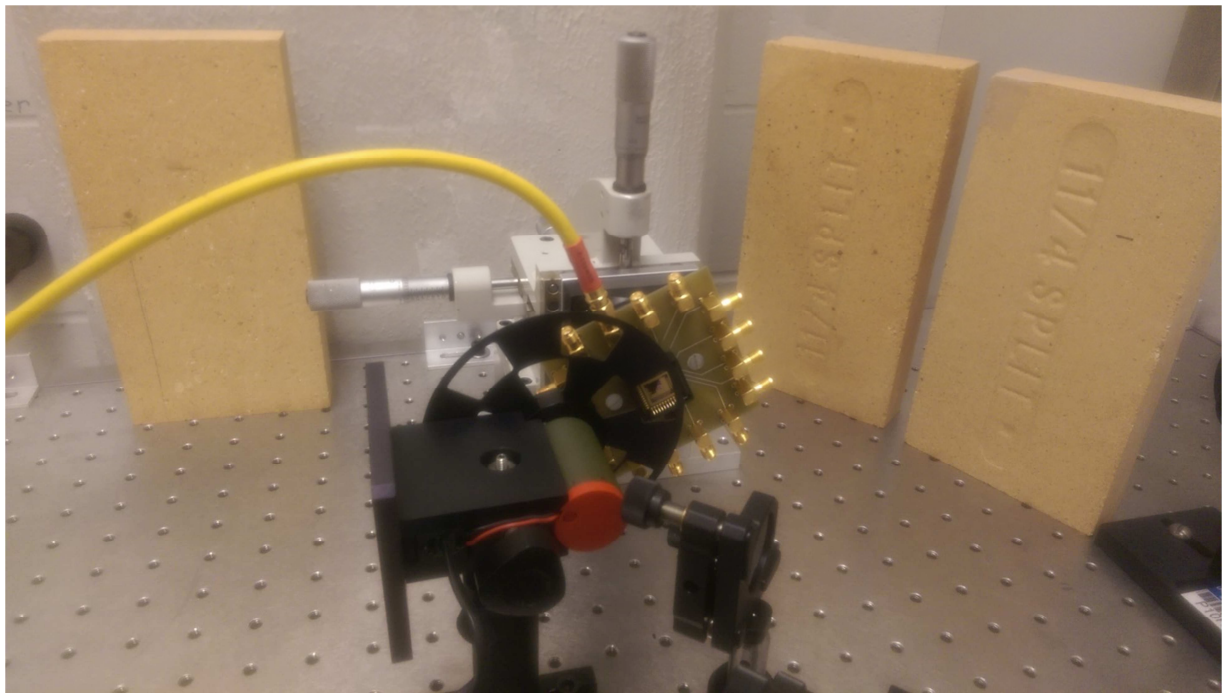

Figure 8. ACMIM diode PCB mounted on micropositioner stage.

3. Device Characterization

3.1 DC Characterization

DC measurements of the device are done using DC needle probes an Alessi probe station. The probes make contact with the ACMIM diode by lightly scratching the contact pads. The probes are connected to an Agilent 5270A parametric measurement mainframe which contains four stimulus and measurement units (SMUs). Two of these SMUs can be used to measure I-V characteristics of a given ACMIM diode. In the characterization of ACMIM diodes, the devices can be classified into three groups: open, short, and diode. An open device is characterized by very low, bias-independent current. This means that either the top and bottom metal layers do not overlap or the oxide layer is too thick to allow current to pass through. A short can be attributed to complete or partial lack of oxide on the bottom metal layer, allowing regions of direct contact between the top and bottom metal layers. The result is an I-V curve with linear voltage dependence near zero bias. This is the most prevalent mechanism of device failure. A diode shows exponential I-V dependence as discussed in Chapter 1.

Figures 9 and 10 show typical I-V curves of ACMIM diodes with applied bias between -0.5V and 0.5V. The resulting currents show perfect exponential behavior in the nA range. The currents for devices oxidized for 45s are lower, indicating a thicker oxide barrier had been formed. It should be noted that symmetry of the I-V curves is due to the fact that the same metal was used for top and bottom metal layers, creating an identical barrier height on both sides of the oxide under equilibrium conditions.
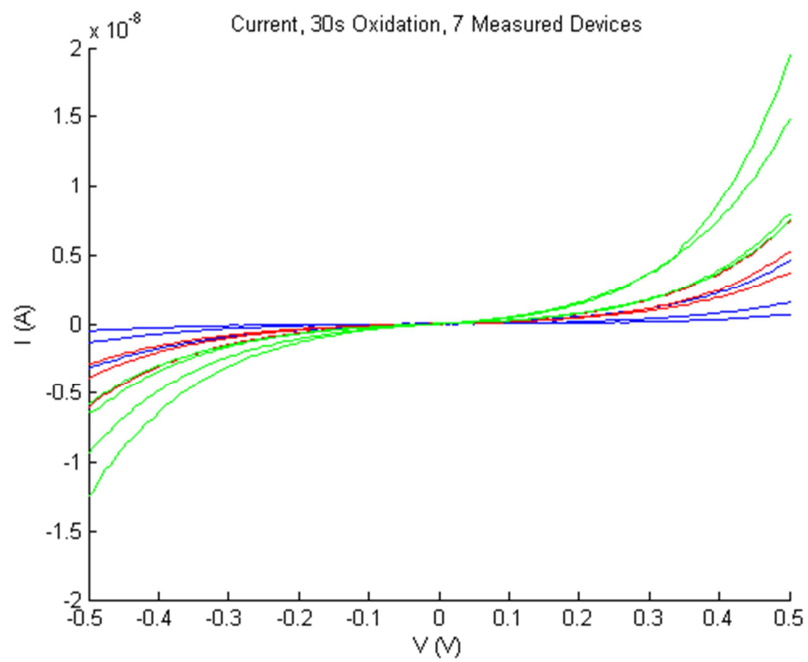
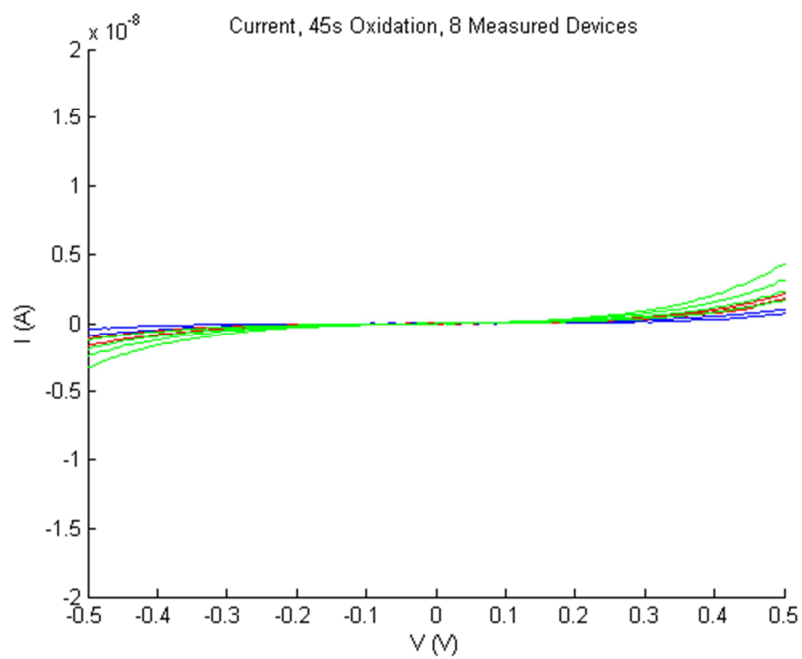**Figure 9. I-V curves of ACMIM diodes with 30s of plasma oxidation.**

Figure 10. I-V curves of ACMIM diodes with 30s of plasma oxidation.

3.2 IR Response Characterization

In this section, the IR response characterization procedure is described. Figure 11 shows a block diagram of the IR measurement setup.
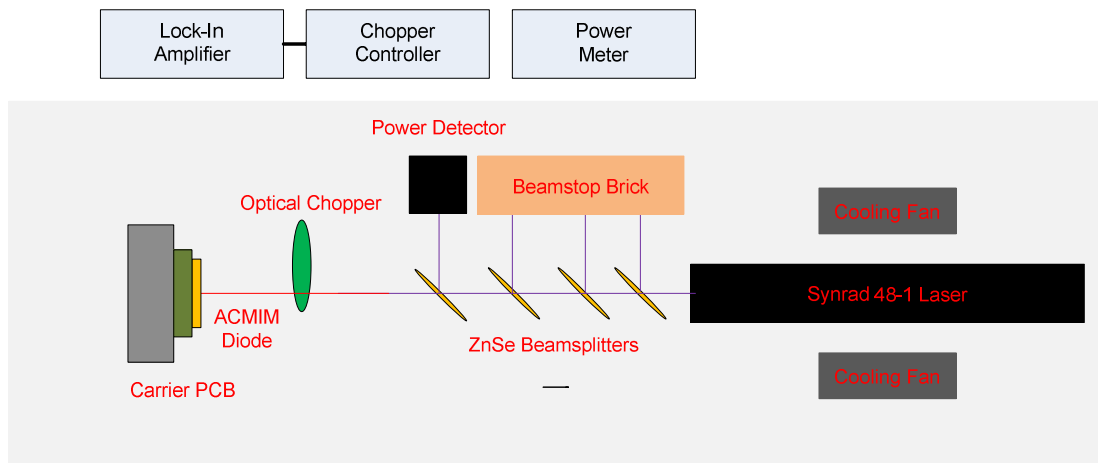
Figure 11. Block diagram of IR measurement setup.

3.2.1 Light Source

Since ACMIM diode's antenna is designed to operate at a wavelength of 10.6μm, a constant light source that operates at that wavelength is required. In this case, a Synrad 48-1 10W CO_2 laser is used. The laser outputs a beam of 10.6 μm wavelength in continuous wave (CW) mode, linearly polarized in the vertical direction. Two fans each providing 250 CFM of air flow are used to provide cooling for the laser. The beam requires an attenuation scheme as the full 10W of CW power can potentially damage the sample and the carrier. Four ZnSe beamsplitters were used in series, each providing roughly a 48%/52% transmission/reflection ratio at 45 degree incidence. At each junction, the beam power is measured using a thermopile detector and a Nova II power meter from Ophir Photonics. Stray beams are directed to beamstop bricks for safe dissipation. At the very end, the final output powers are measured to be 0.5W/0.48W. Because the ratio of transmission and reflection out of the

final beamsplitter is constant, the beam power incident on the measured ACMIM diode can be determined by monitoring the reflected beam from the final beamsplitter.

Another important aspect of the light source is the shape or spatial profile of the beam. The thermopile detector is a large area detector and it can only determine the total power contained in the beam, but not its distribution in space. Ideally, we want the beam to have uniform power distribution in our area of interest, but this may not be the case. Exact characterization of the beam requires a camera-based profiler with a pyroelectric array which is expensive and impractical for research purposes. Another alternative is the knife edge scan measurement [10]. With the thermopile detector monitoring the output of the laser, a piece of metal is scanned in constant increments such that the beam goes from fully blocked to fully exposed. The amount of power detected by the detector represents the partial power contribution for the partially blocked beam. This can be used to fit a Gaussian function to the beam power. The procedure was done in both the x and y directions to get a 2D spatial map of the beam profile. The measurement Gaussian fit to the measured beam profile is shown in Figure 12. The plots show that the beam power stays within 95% in a circle of 1mm diameter around the center of the beam. Since the distance between the farthest devices in the array is 0.5mm, we can measure multiple devices without having to readjust the x and y positions of the stage.
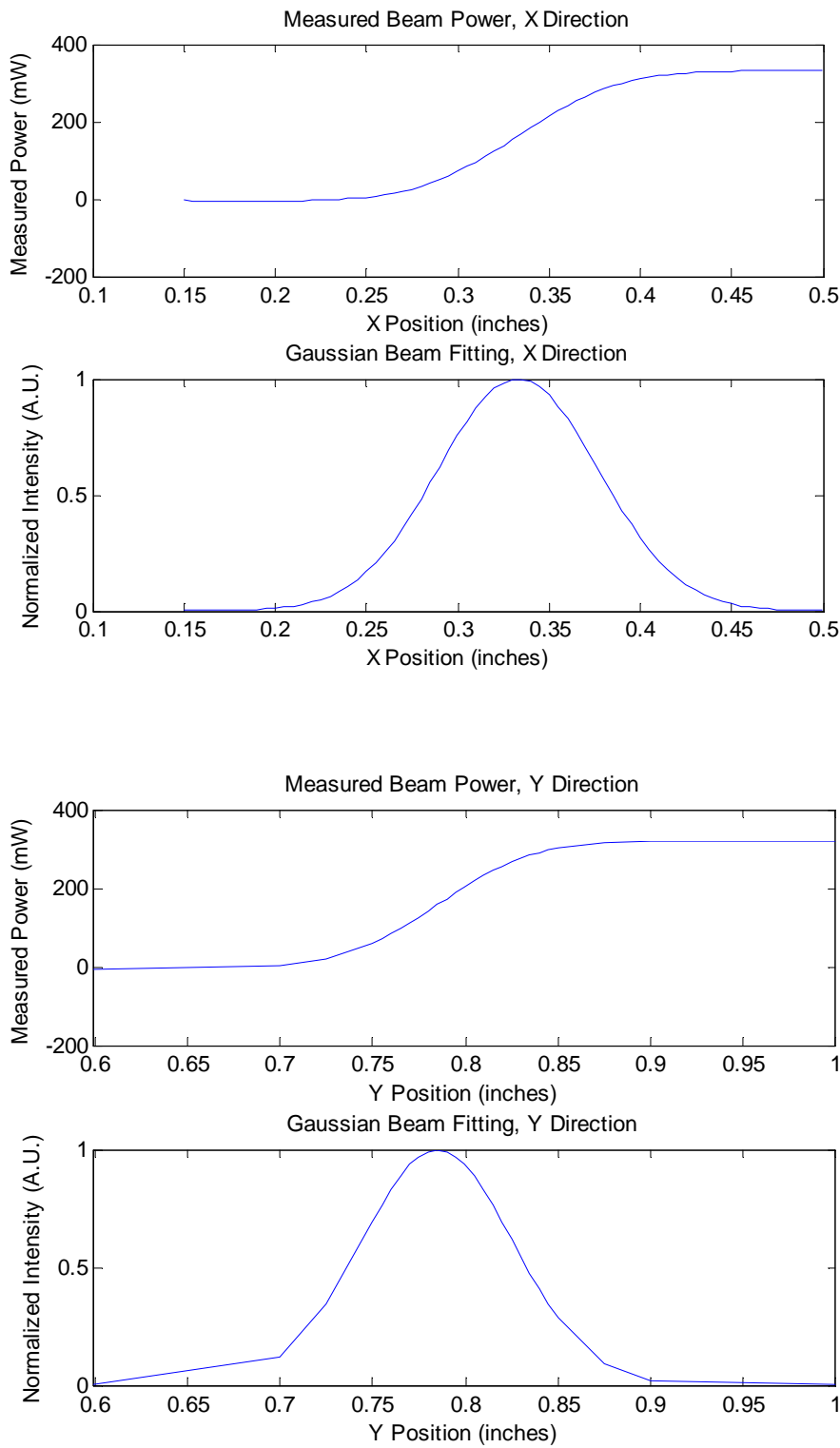
Figure 12. Measured power and gaussian beam fitting of the laser profile in the X and Y directions.

3.2.2 Lock-in Measurement

From DC I-V measurements, we know that the device current is in the nA range with several hundred mV of bias applied. In an IR measurement configuration, the AC voltage generated between the two bowties as a result of the IR irradiation is likely to be much smaller and thus the resulting current is much smaller. Such a weak signal can easily be overwhelmed in the presence of noise. One practical workaround to this conundrum is the lock-in method. It involves the modulation of the signal at a specific frequency ω such that the total current is simply the modulated signal plus a noise current.

$$I_{total}(t) = I_{signal}(t)cos(\omega t) + I_{noise}(t) \tag{2}$$

$$I_{received}(t) = I_{signal}(t)cos^2(\omega t) + I_{noise}(t)\cos(\omega t) \tag{3}$$

$$I_{received}(t) = I_{signal}(t)(0.5 + 0.5cos(2\omega t)) + I_{noise}(t)\cos(\omega t) \tag{4}$$

At the receiving end, the signal is mixed with a cosine wave of the same frequency as the modulation signal. When two cosine waves of equal frequency ω are multiplied together, the result is a DC component and a component at 2ω. All other signals are modulated by ω. Since the only true DC component comes from the signal current, the signal can be isolated using an appropriate low-pass filter.

A Stanford Research Systems SR540 Optical Chopper is used to modulate the laser beam at 400Hz, thus modulating the DC response current. The signal goes to a Stanford Research Systems SR570 Low Noise Current Preamplifier. This current preamplifier is a transimpedance amplifier that transforms the output current to an output voltage with a gain of 10^6 V/A. Finally, the output voltage goes into the SR830 DSP Lock-In Amplifier where signal is multiplied by a 400Hz reference signal from the SR540

Optical Chopper and selectable low-pass filters are applied. Figure 13 shows the SR570 and SR830, and

Figure 14 shows the final optical layout for the IR measurement. The setup is contained in a

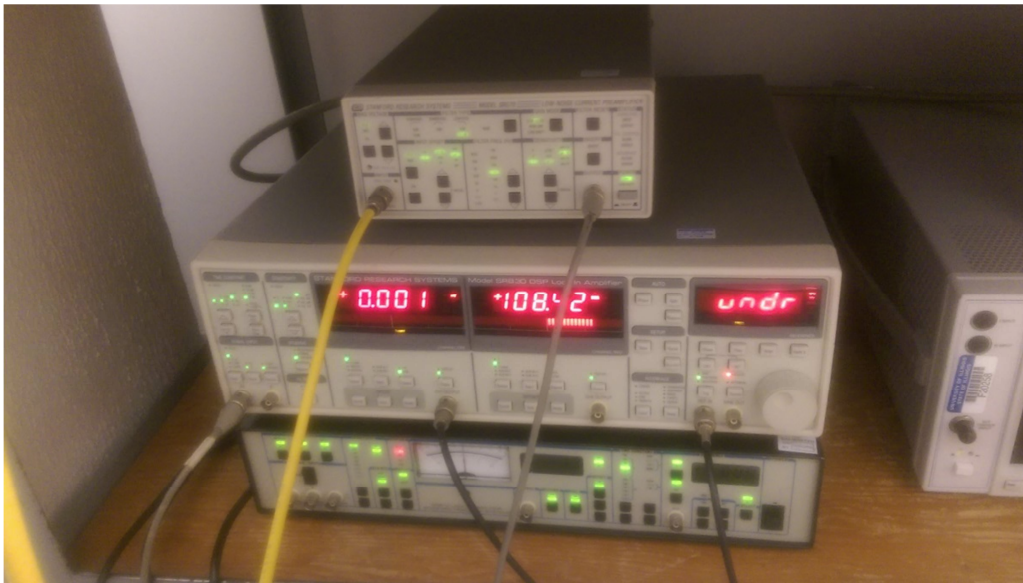Polycarbonate box to contain any stray reflections.

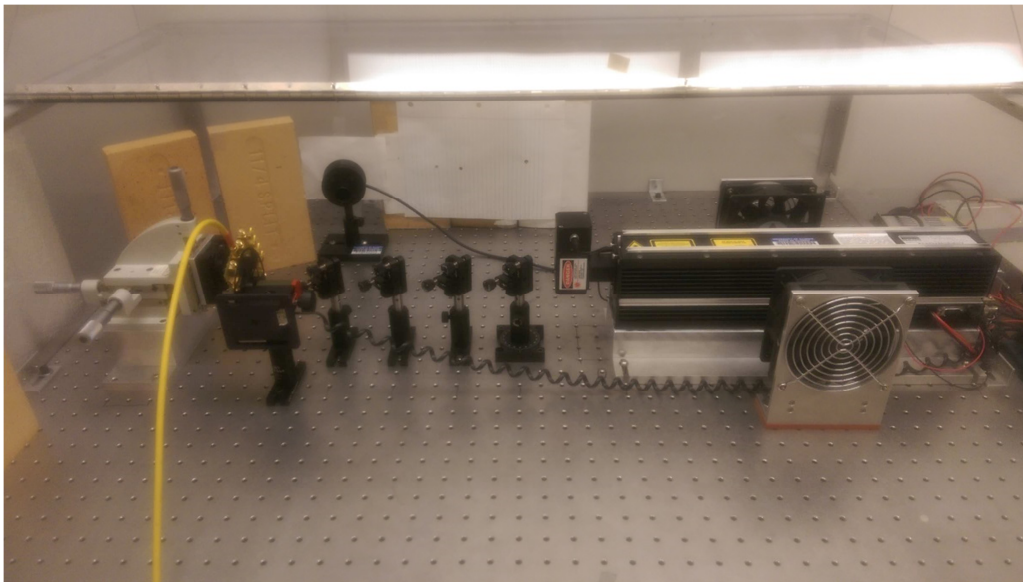Figure 13. SR570 current preamplifier and SR830 lock-in amplifier.

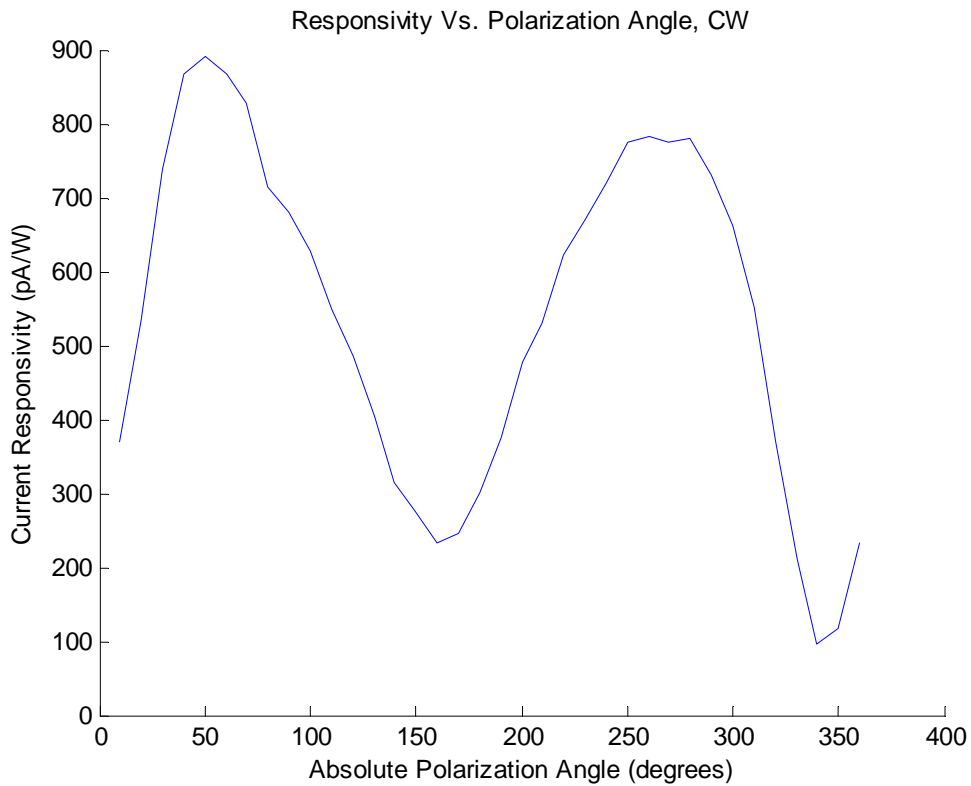Figure 14. Final optical layout for IR measurement setup.

Figure 15. Current responsivity of the ACMIM diode as a function of device rotation.

The current output from the lock-in amplifier is measured while the laser power is monitored.

The measurement is taken as the device is rotated from 0 to 350 degrees in 10 degree increments and

the current responsivity (A/W) is calculated. The current output is expected to be the sum of a field-

assisted tunneling component and a thermal component. As the device is rotated, the ACMIM diode

antenna's alignment to the laser beam is swept from maximum to minimum. As a result, the AC bias on

the ACMIM diode is modulated and the current is expected to yield a response that varies with the

cosine squared of the polarization angle. On the other hand, since the thermal component is

polarization-independent, it is expected to stay constant. The responsivity plot shown in Figure 15

shows clear peaks and valleys and a sharp dependence on the polarization angle, indicating that the

majority of the DC current comes from the field assisted tunneling mechanism. The discrepancy from a pure cosine likely comes from sub-optimal device positioning as the sample is rotated.

4. Conclusion and Future Work

In this work, Ni-NiO-Ni ACMIM diodes were fabricated. The devices show clear exponential DC I-V behavior. The current responsivity of the device varies sharply as a function of the polarization response, indicating a conduction mechanism dominated by field-assisted tunneling. Several improvements can be made concerning device characterization in the future. First, the addition of a rotating half-wave plate should help in getting a cleaner polarization dependence measurement as the ACMIM diode can be kept in a fixed position while the polarization angle is varied. Second, the detectivity or the D* of the device can be determined to provide a baseline comparison to other detectors. D* is a metric that gives the signal-to-noise ratio (SNR) of a specific detector under 1 W of incident power with a 1 cm^2 effective detector area and measured with 1 Hz of noise bandwidth.

$$D^* = \frac{\sqrt{A_d \Delta f}}{NEP} \tag{5}$$

A_d is the detector effective area determined using a deconvolution procedure similar to [10], Δf is the noise measurement bandwidth, and NEP is the noise equivalent power defined as the ratio between total received power or radiant flux and the SNR of the detector.

$$NEP = \frac{P_e}{SNR} = \frac{E_e A_d}{\frac{I_S}{I_N}} \tag{6}$$

The SNR of the device is the ratio between the signal and noise currents in the detector and can be characterized using a spectrum analyzer. E_e is the illumination intensity determined from beam profiling.

References

[1] K. Choi, F. Yesilkoy, G. Ryu, S. H. Cho, N. Goldsman, M. Dagenais, and M. Peckerar, "A focused asymmetric metal-insulator-metal tunneling diode: fabrication, DC characteristics and RF rectification analysis," *IEEE Transactions on Electron Devices*, vol. 58, no. 10, pp. 3519-3528, Oct. 2011.

[2] M. Heiblum, S. Wang, J.R. Whinnery, and T. Gustafson, "Characteristics of integrated MOM junctions at DC and at optical frequencies," *Quantum Electronics, IEEE Journal of*, vol. 14, no. 3, pp. 159-169, March 1978.

[3] M. Nagae, "Response time of metal-insulator-metal tunnel junctions," *Japanese Journal of Applied Physics*, vol. 11, no. 11, pp. 1611-1621, 1972.

[4] J.W. Dees, "Detection and harmonic generation in the submillimeter wavelength region," *Microwave Journal*, vol. 9, pp. 48-55, 1966.

[5] M. Heiblum, S. Y. Wang, T. K. Gustafson, and J. R. Whinnery, "Edge-MOM diode: an integrated, optical, nonlinear device," *IEEE Transactions on Electron Devices*, vol. ED-24, p. 1199, 1977.

[6] C. Fumeaux, J. Alda, and G. D. Boreman, "Lithographic antennas at visible frequencies," *OSA Optics Letters*, vol. 24, pp. 1629-1631, 1999.

[7] J. A. Bean, A. Weeks, and G. D. Boreman, "Performance optimization of antenna coupled tunnel diode infrared detectors," *IEEE Journal of Quantum Electronics*, vol. 47, no. 1, pp. 126-135, Jan. 2011.

[8] J.A. Bean, "Thermal infrared detection using antenna-coupled metal-oxide-metal diodes," Ph.D. dissertation, U of Notre Dame, 2008.

[9] F. Yesilkoy, "IR detection and energy harvesting using antenna coupled MIM tunnel diodes," Ph.D. dissertation, U of Maryland, 2012.

[10] J. Alda, C. Fumeaux, I. Codreanu, J. A. Schaefer, and G.D. Boreman, "Deconvolution method for two-dimensional spatial-response mapping of lithographic infrared antennas," *OSA Applied Optics Journal*, vol. 38, pp. 3993-4000, 1999.